Proceedings of the Thirty-second (2022) International Ocean and Polar Engineering Conference **www.isope.org**
Shanghai, China, June 5–10, 2022

ISBN 978-1-880653-81-4; ISSN 1098-6189

Study of a Free-Flooding Anti-Motion Structure of the Cylindrical FPSO

Weinan Hao[1], *Zhiyuan Wei*[2], *Decheng Wan*[1*]

[1]Computational Marine Hydrodynamic Lab (CMHL), School of Naval Architecture, Ocean and Civil Engineering,
Shanghai Jiao Tong University, Shanghai, China
[2]Marine Design and Research Institute of China, Shanghai, China
*Corresponding author

ABSTRACT

Anti-motion structures are commonly used to improve motion performance of cylindrical FPSO. In present work, the self-developed naoe-FOAM-SJTU solver, which was validated by comparing numerical and experimental results, was used. The effects of the free-flooding anti-motion structure on heave natural period and damping performance of the FPSO were studied by two methods of free decay and forced motion. The results show that the free-flooding structure has little effect on heave natural period, but the damping coefficient can be significantly increased due to the generation of vortices around the structure and in the internal fluid due to the opening.

KEY WORDS: Cylindrical FPSO; anti-motion structure; naoe-FOAM-SJTU; natural period; damping performance; free heave decay; forced heave motion.

INTRODUCTION

Cylindrical floating production storage and offloading system (FPSO) has many advantages, but its heave motion performance is poor (Ji, Li, Tang and Tong, 2019). It is often used to install an anti-motion structure in the lower part of the FPSO main cylinder body to improve movement (Ji, Li, Tang and Tong, 2019; Ji, Li, Tang, Zhu and Hu, 2019).

In present work, the effects of the free-flooding anti-motion structure on heave natural period and damping performance of the FPSO were studied by two methods of free decay and forced motion, which are commonly used to determine the hydrodynamic performance (Rao, Seeninaidu and Bhattacharyya, 2014; Igbadumhe, Sallam, Fürth and Feng, 2020).

Free Heave Decay

Under the assumption of linear damping, the equation of free heave decay can be given as

$$\left(m+m_a\right)\ddot{z}(t)+b\dot{z}(t)+cz(t)=0 \tag{1}$$

where m is mass of FPSO, m_a is heave added mass, b is the damping coefficient, and c is the restoring stiffness coefficient. $z(t)$, $\dot{z}(t)$ and $\ddot{z}(t)$ are the displacement, velocity and acceleration in heave direction respectively. in the case of small-amplitude motion, the water plane of the cylindrical FPSO is a circle, and the area of water plane A_w is constant, which is defined in Eq. 2

$$A_w = \pi D^2 / 4 \tag{2}$$

where D is the diameter of the water plane. So that c can be written as

$$c = \gamma A_w \tag{3}$$

where

$$\gamma = \rho g \tag{4}$$

In Eq. 4, ρ and g are respectively the density of water and the acceleration due to gravity.

Given the known parameters in Eq. 1, heave natural period T and the dimensionless damping coefficient d are defined in Eq. 5 and Eq. 6 respectively.

$$T = 2\pi\sqrt{\frac{m+m_a}{c}} \tag{5}$$

$$d = \frac{b}{2\sqrt{\left(m+m_a\right)c}} \tag{6}$$

If z_n denotes the positive heave amplitude of the *n*th oscillation in heave decay curve, which is shown in Fig. 1, under the assumption of linear damping, d can be obtained from Eq. 7, where z_{n-1} and z_n are the heave amplitudes of adjacent half-periods, and $z_{n-1} > z_n$.

$$d = \frac{1}{\pi} \ln \left| \frac{z_{n-1}}{z_n} \right| \tag{7}$$

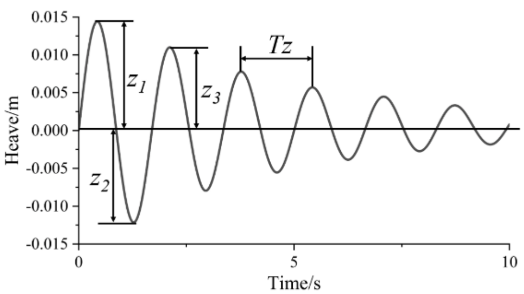

Fig. 1 Heave decay curve.

Forced Heave Motion

It was noted (Avalos and Wanderley, 2018; Ji, Li, Tang and Tong, 2019) that the hydrodynamic coefficients are acquired from CFD simulation results. Assuming that the body is oscillating harmonically, in heave motion, $z(t)$, $\dot{z}(t)$ and $\ddot{z}(t)$ are written as

$$\begin{cases} z(t) = A\sin(\omega t) \\ \dot{z}(t) = A\omega\cos(\omega t) \\ \ddot{z}(t) = -A\omega^2\sin(\omega t) \end{cases} \tag{8}$$

where the motion amplitude of the structure is A, the movement frequency is ω. The hydrodynamic force F applied on the structure can be obtained at each time step. Assuming a linear damping coefficient, the hydrodynamic load meets the Eq. 9,

$$m_a\ddot{z}(t) + b\dot{z}(t) + cz(t) + F = 0 \tag{9}$$

For a sinusoidal signal, F is given by Eq. 10,

$$F = F_0 \sin(\omega t + \varphi) \tag{10}$$

where F_0 is the load amplitude, φ is the phase angle.

Inserting Eq. 8 and Eq. 10 in Eq. 9, and substituting Eq. 9, the equation becomes Eq. 11 and Eq. 12. Hereby, the added mass m_a and the damping coefficient b can be written as Eq. 13 and Eq. 14. From Eq. 6, the dimensionless damping coefficient d can be determined.

$$\begin{aligned} &F_0\cos(\varphi)\sin(\omega t) + F_0\sin(\varphi)\cos(\omega t) \\ &= (m_a\omega^2 - c)A\sin(\omega t) - b\omega A\cos(\omega t) \end{aligned} \tag{11}$$

$$\begin{aligned} &\left[F_0\cos(\varphi) - (m_a\omega^2 - c)A\right]\sin(\omega t) \\ &+\left[F_0\sin(\varphi) + b\omega A\right]\cos(\omega t) = 0 \end{aligned} \tag{12}$$

$$m_a = \frac{F_0\cos(\varphi) + cA}{A\omega^2} \tag{13}$$

$$b = -\frac{F_0\sin(\varphi)}{A\omega} \tag{14}$$

NUMERICAL METHODS

Governing Equations

The CFD solver naoe-FOAM-SJTU solves the unsteady fluid of viscous incompressible, the governing equations are as follows (Liu, Zhao and Wan, 2021; Wu, Wang and Wan, 2021):

$$\nabla \cdot \mathbf{U} = 0 \tag{15}$$

$$\begin{aligned} &\frac{\partial \rho \mathbf{U}}{\partial t} + \nabla \cdot (\rho \mathbf{U}\mathbf{U}) = \\ &-\nabla p_d - \mathbf{g}\cdot\mathbf{x}\nabla\rho + \nabla\cdot(\mu\nabla\mathbf{U}) \end{aligned} \tag{16}$$

where $\mathbf{U}$ is the velocity field, μ is the dynamic viscosity. p_d is the dynamic pressure, which is defined as Eq. 17. And p is the total pressure.

$$p_d = p - \rho\mathbf{g}\cdot\mathbf{x} \tag{17}$$

Free Surface Treatment

The calculation of the two-phase flow of floating structures is a serious problem, and the treatment of the free surface is quite critical. The solver uses the volume of fluid method (VOF) to capture the free surface (Liu, Zhao and Wan, 2021; Wu, Wang and Wan, 2021), which can handle numerical dissipation well and has high accuracy.

Sponge Layer

In the numerical calculation, when the wave propagates to the exit boundary of the calculation domain, the wave reflection phenomenon will appear. To avoid wave reflection, a sponge layer (Liu, Zhao and Wan, 2021) is set at the outlet of the computational domain, as shown in Fig. 2.

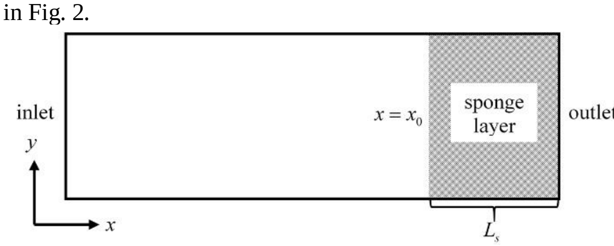

Fig. 2 Sponge layer.

Discretization Schemes

There are several built-in numerical schemes in OpenFOAM for the numerical approximation of the PDE terms in the governing equations Eqs. 15~16. An overview of the discretization schemes used in this work is given in Table 1.

Table 1. The discretization of PDE terms

	Term	Discretization
Temporal Schemes	ddtSchemes	CrankNicolson 0.9
gradSchemes	default	Gauss linear
divSchemes	div(rhoPhi, U)	Gauss linearUpwind grad(U)
	div(phi, alpha)	Gauss PLIC interfaceCompression vanLeer 1
	div(phirb, alpha)	Gauss linear
laplacianSchemes	default	Gauss linear corrected
interpolationSchemes	default	linear
snGradSchemes	default	corrected

Dynamic Mesh Deformation Technology

After the movement of the body is obtained, its position in the computational domain needs to be updated, and the positions of other grids should also match the movement of the boundary of the body. The solver uses dynamic mesh deformation technology. When the boundary of the body changes, the cell shape is changed by displacing the grid points, and the number of grids and the topological relationship are not adjusted.

NUMERICAL VALIDATION

In order to validate the solver used in this work, the numerical result was compared to experimental result of Huang et al (Huang, Wang and Zhao, 2017). The cylindrical FPSO scaled at a ratio of 1:82.5, based on Froude scaling was chosen for study. The detailed dimensions of the structure are described in Table 2 and the overview of the model M0 is shown in Fig. 3.

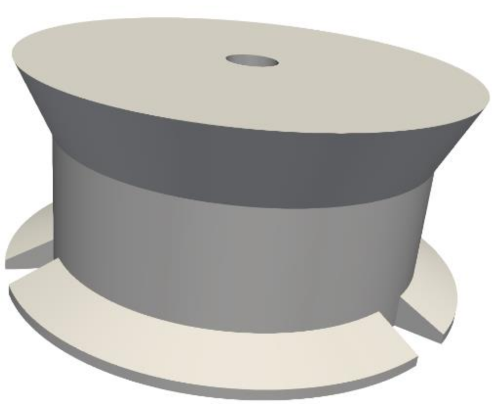

Fig. 3 Overview of the model (M0).

Table 2. Main characteristics of M0

Parameters	Prototype	Model test (1:82.5)
Diameter of the main body (m)	88	1.067
Diameter of the moonpool (m)	12	0.145
Diameter of the anti-motion structure (m)	110	1.333
Draft (m)	32	0.388
Mass (t)	208548.8	0.366
Center of gravity (m)	24.09	0.292

Computational Domain

The Cartesian coordinate system was established with the center of the model at the water plane as the origin, and the coordinate system followed the right-hand rule. A computational domain was established under this coordinate system. The domain extended to $-8m \le x \le 8m$, $-8m \le y \le 8m$, $-5m \le z \le 2m$. Fig. 4 shows that the domain was divided into two parts by the free surface plane. The upper part is the air phase and the lower part is the water phase. The length of sponge layer was set as 2 m.

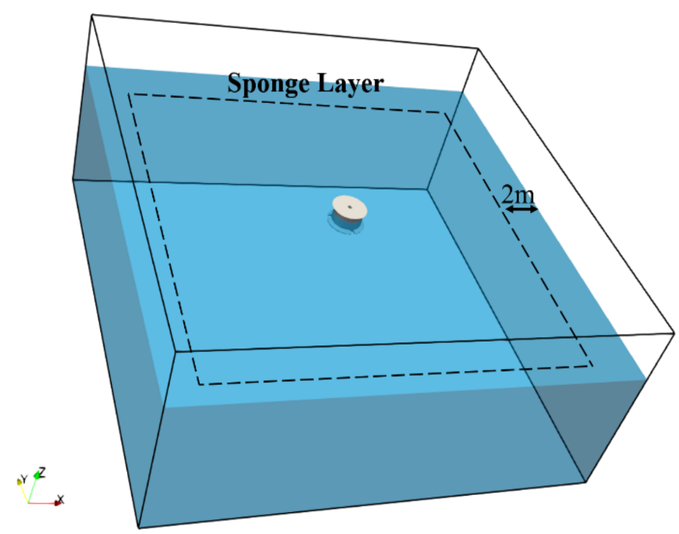

Fig. 4 Computational domain.

In present study, blockMesh and snappyHexMesh tools were used to generate grids. Fig. 5 shows the mesh size distribution around the model. Considering the complicated model surface, hybrid mesh was used, so that mesh can adhere to the surface accurately. The mesh size distribution was made finer near the free surface and the anti-motion structure, and coarser outwards to obtain better resolution of the flow parameters like velocity and pressure near the model. As shown in Fig. 5, the figures displayed represent refinement level, and level 0 indicates the basic background mesh size. The total number of cells used for simulation was 1.6 million. The time step was 0.001s.

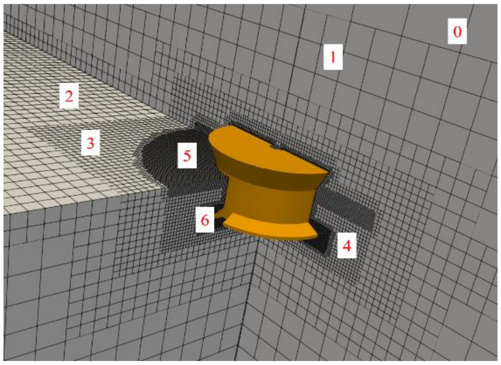

Fig. 5 Mesh size distribution.

Results

The heave decay curve of M0 obtained by numerical simulation and the result after fast Fourier transform (FFT) are shown in Fig. 6 and Fig. 7, respectively.

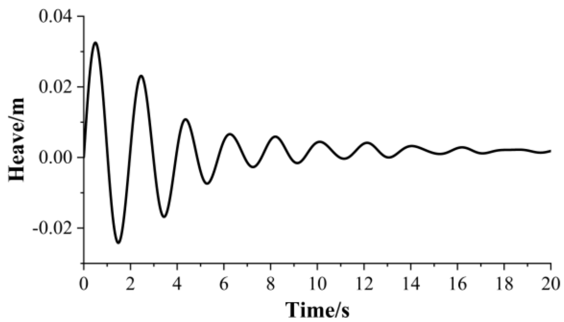

Fig.6 Heave decay curve of M0.

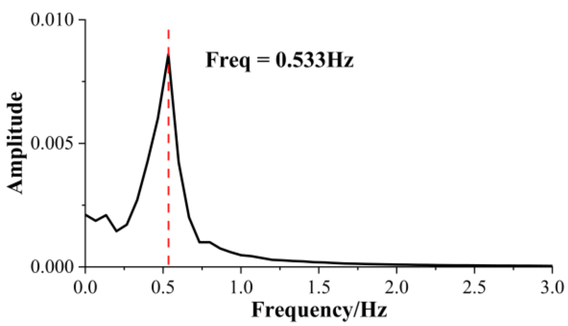

Fig.7 FFT result of M0.

Table 3. Heave natural period results comparison

	Heave Natural Period
experimental result (s)	17.221
numerical result(s)	17.031
Relative error (%)	1.10

The numerical results of heave natural period of M0 are compared with the experimental result, as shown in Table 3. It can be seen that two results for Heave natural period are in good agreement.

FREE-FLOODING ANTI-MOTION STRUCTURE

The cylindrical FPSO model with free-flooding anti-motion structure is numbered M1. At free-flooding anti-motion structure, damping holes are opened on the upper and lower plates of the anti-motion structure to communicate with seawater, as shown in Fig. 8 and Fig. 9. The centers of the holes at the upper and lower are not on the same line in the vertical direction (Ji, Li, Tang, Zhu and Hu, 2019), so that the fluid will form turbulence in the process of entering and leaving the orifice, thereby increasing damping.
The mesh size distribution around the model was consistent with M0, and high-level refinement was performed around the holes to achieve capture accuracy, as shown in Fig. 10 and Fig. 11. The total number of cells was 3.27 million.
With the same main dimensions such as draft, the external diameter and the main body of M0, the displacement of M1 is 342.482kg.

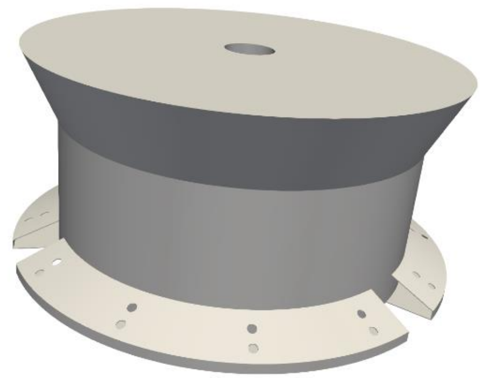

Fig. 8 Overview of the model (M1).

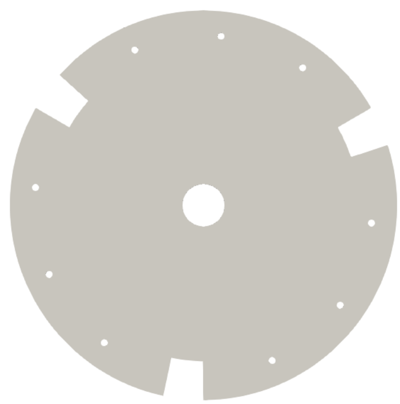

Fig. 9 Lower plate of M1.

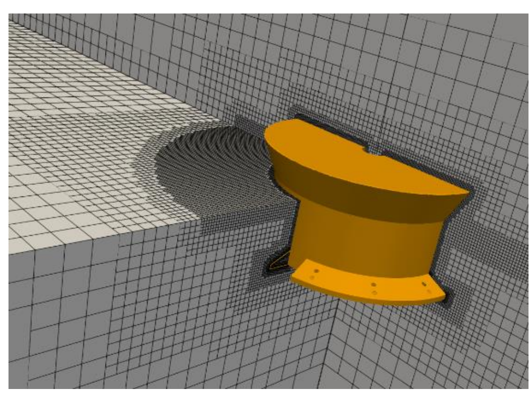

Fig. 10 Mesh size distribution of M1.

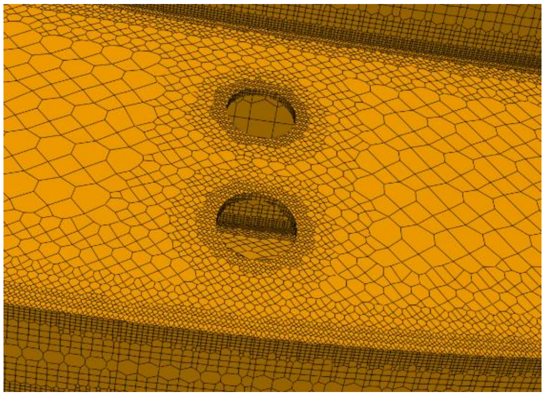

Fig. 11 Grid refinement around holes.

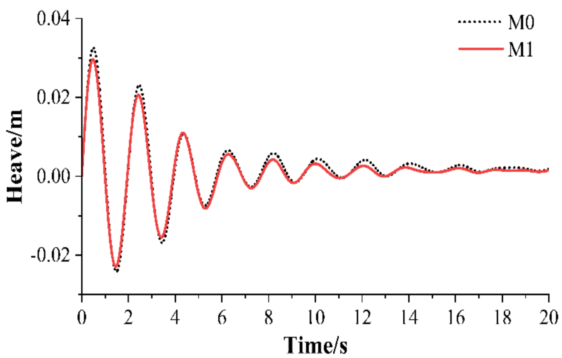

Fig. 12 Comparison of heave decay curves of M0 and M1.

Fig. 12 shows the heave decay curves of M0 and M1 with same initial velocity. The heave natural periods obtained through FFT are almost no difference between each other. However, it can be seen that opening holes on the anti-motion structure to make it open to the sea can significantly improve the damping performance because of the heave amplitudes are clearly decreased.

Ignoring the effect of damping on the natural period, the period T of the FPSO can be obtained as Eq. 5. The anti-motion structure is free-flooding, so that m of M0 decreases by Δm, and m_a of M0 increases by Δm_a. But the two increments are roughly the same, so that $m+m_a$ of M1 has little difference from that of M0.

The dimensionless damping coefficients d is obtained according to Eq. 7, and take the average value of first six cycles. The dimensionless damping coefficients of M0 and M1 are 0.069 and 0.079, respectively.

FORCED HEAVE MOTION

The FPSO under investigation is similar to the Spar platforms which have the configuration of a cylinder with heave plate. As a result, the nondimensional characteristic parameter which represents the amplitude can be defined as

$$KC = \pi A / R \tag{18}$$

where R is the diameter of the anti-motion structure. Since the damping effect and added mass of Spar are related to the KC number (Keulegan Carpenter number) and oscillation frequency (Rao, et al, 2014), and the damping coefficient of the cylindrical FPSO is also related to the KC number (Ji, Li, Tang and Tong, 2019), therefore, in the numerical simulation of forced heave motion, the two models of M0 and M1 take the same KC number and frequency. It is observed that the first amplitudes of the two decay curves in Fig. 12 are both around 0.03 m, and the two have almost the same heave natural period. So that A is 0.03 and ω is 3.35, which values are taken for Eq. 8.

In this work, where the signal is not sinusoidal, F_0 and φ are obtained through a first order Fourier analysis (Avalos and Wanderley, 2018) as follows

$$F = F_0 \sin(\omega t + \varphi) + C_0 \tag{19}$$

The parameters obtained by the two models and the results of the related formulas are shown in Table 4.

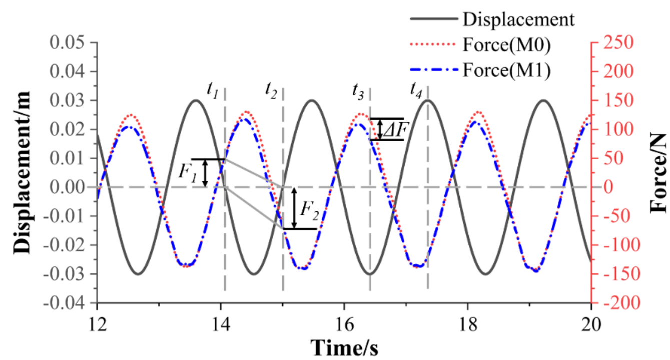

Fig. 13 Force and displacement curves of M0 and M1.

As shown in Table 4, the natural periods corresponding to the two models are obtained, which are 17.251s and 17.185s respectively. It is obvious that they are almost the same.

By the results of the two methods, the free-flooding anti-motion structure has little effect on the natural period of the heave motion of the cylindrical FPSO, but has a significant effect on the damping of the motion. Comparing the damping coefficients calculated by the two methods, the results obtained from the decay curves are smaller. But both show that the free-flooding structure can make damping increase.

As shown in Fig. 13, at t_1, t_2, $\sin(\omega t) = 0$, $\cos(\omega t) = 1$, and the force applied on the two models are almost identical. According to Eq. 11, at these moments,

$$F = -b\omega A \tag{20}$$

Fig. 13 shows that F_1 is less than F_2, that is, the damping generated when the FPSO moves upward is larger than that when it moves downward. Referring to the data in Table 4, the magnitude of the constant term C_0 in the Fourier analysis may reflect the asymmetry of force caused by the movement of the asymmetric structure.

At t_3, t_4, $\sin(\omega t) = 1$, $\cos(\omega t) = 0$. At these moments,

$$F = (m_a \omega^2 - c)A \tag{21}$$

Table 4. Parameters of M0 and M1 under forced heave motion

Parameters	M0	M1
ω (rad/s)	3.35	3.35
A(m)	0.03	0.03
F_0 (N)	131.002	131.002
φ (rad)	-2.668	-2.578
C_0 (N)	-5.645	-13.502
A_w (m^2)	0.894	0.894
c (N/m)	8766.300	8766.300
m (kg)	366.456	342.482
m_a (kg)	434.538	452.389
$m+m_a$ (kg)	800.994	794.871
b (N*s/m)	594.642	696.830
d	0.112	0.132
T (s)	17.251	17.185

At t_4, the two curves are almost the same. At t_3, force of M0 is more than M1. The value of ΔF in Fig. 13 is determined by the difference in the added mass m_a of the two models. At the same time, the difference of the hydrodynamic force curves is mainly concentrated in the half cycle when the FPSO motion displacement is below the equilibrium position. The possible reason is that when the displacement is above the equilibrium position, the performance of the two models in the added mass is not much different due to the restriction of the free surface; when it is below the equilibrium position, the restriction effect of the free surface is insignificant, which makes the added mass differences manifested.

FLOW FIELD ANALYSIS

As shown in Fig. 14, four moments of 0.25, 0.5, 0.75, and 1 T in a steady motion cycle of forced motion are selected to analyze the flow field around the anti-motion structures of two models.

Vorticity Contours of M0

The section with y direction as the normal is taken for vorticity analysis. The heaving motion of M0 is mainly caused by the separation of the boundary layers at the upper and lower edges of the anti-motion structure, forming a vortex. It can be seen from the vorticity contours (Fig. 15) at 0.25 T and 0.5 T that when M0 moves upward, the upper edge completes a complete vortex shedding. At the same time, the boundary layer at the lower edge begins to separate, but is cut off by the vorticity at the upper edge, and the complete vortex shedding is not completed. During the whole cycle, vorticity near the upper edge of the structure is always significant and large. Besides, obvious vorticity can be seen in the upper left corner of the figure, while the vorticity in the lower right corner is around 0. Because the cylindrical FPSO is a shallow draft structure, the interaction between the motion and the free surface has a significant impact on the flow field in the range of draft, and also leads to the asymmetric phenomenon of vortex leakage at the upper and lower edges of the anti-motion structure.

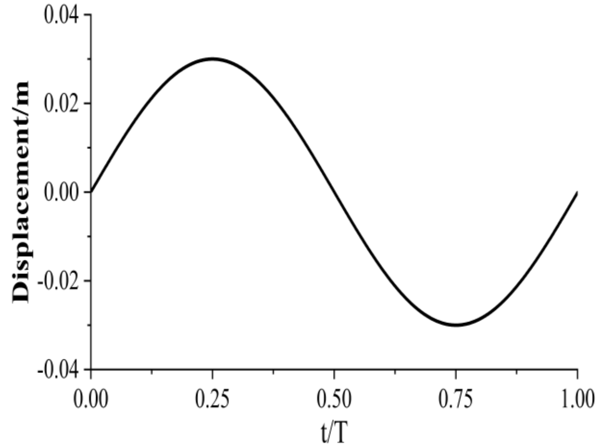

Fig. 14 A steady motion cycle of forced motion.

Velocity Field of M1

Due to the dislocation of the upper and lower holes of the anti-motion structure, this work takes the same moment to make cross-sections at the upper and lower holes respectively, as shown in Fig. 16, and analyzes the velocity field around the structure. From the velocity distribution around holes, the velocity directions of the upper and lower openings are the same and opposite to the movement direction. That is, when M1 moves upward, the water flows in from the upper two holes and flows out from the lower hole, and when M1 moves downward, the water flow direction is exactly opposite.

The streamline distribution is also drawn in Fig. 16, and it can be seen that there are many vortices distributed in the anti-motion structure. These vortices are generated due to the edges of holes, the corners inside the structure, and the water flow caused by opening to the sea. So that the viscous damping in the motion of M1 can also be increased.

CONCLUSIONS

In present work, the self-developed naoe-FOAM-SJTU solver was used in order to study the effects of the free-flooding anti-motion structure on heave natural period and damping performance of the cylindrical FPSO by two methods of free decay and forced motion. It is concluded that the free-flooding structure has little effect on heave natural period, but the damping coefficient can be significantly increased due to the generation of vortices around the structure and in the internal fluid due to the opening.
According to the results of forced heave motion, the damping generated when the FPSO moves upward is larger than that when it moves downward. The influence of change of added mass is mainly obvious when the FPSO motion displacement is below the equilibrium position.
With the analysis of flow field of M0 and M1, because of the shallow draft of cylindrical FPSO, the interaction between the FPSO and the free surface has a significant impact in the range of draft, and also leads to the asymmetric phenomenon of vortex leakage at the upper and lower edges of the anti-motion structure. From the velocity distribution around holes, the velocity directions of the upper and lower openings are the same and opposite to the movement direction.

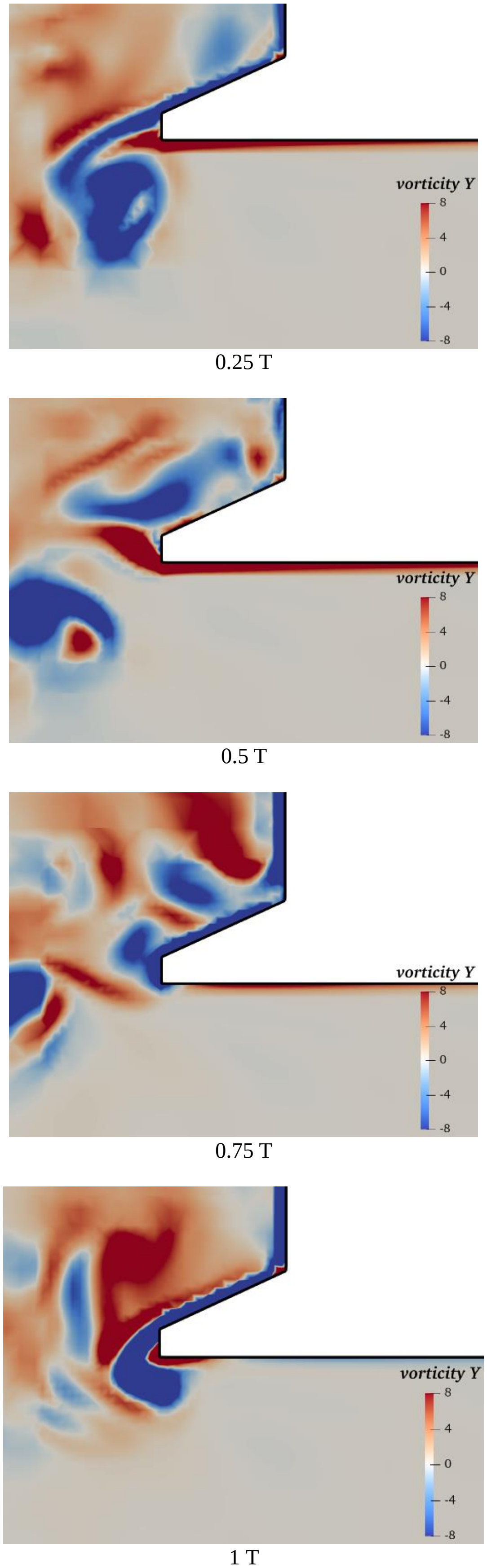

Fig. 15 Vorticity contours of M0.

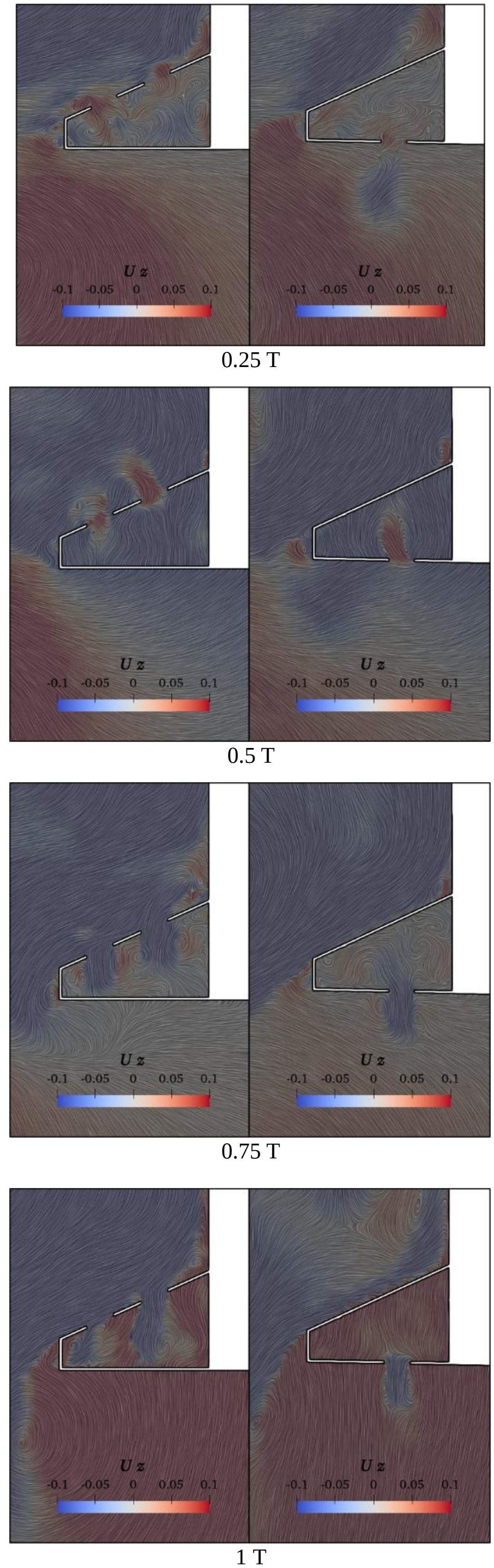

Fig. 16 Velocity field of M1.

ACKNOWLEDGEMENTS

This work was supported by the National Natural Science Foundation of China (51879159, 52131102), and the National Key Research and Development Program of China (2019YFB1704200), to which the authors are most grateful.

REFERENCES

Avalos, GO, and Wanderley, JB (2018). " Numerical study of forced roll oscillation of FPSO with bilge keel," *Ocean Engineering*, 147, 304-317.

Huang, J, Wang, ZH, and Zhao, ZH (2017). “Model experimental research on hydrodynamic performance of cylindrical floating workover production storage offloading (FWPSO),” *The Ocean Engineering*, 35(6), 119-124.

Igbadumhe, JF, Sallam, O, Fürth, M, and Feng, RH (2020). “Experimental determination of non-linear roll damping of an FPSO pure roll coupled with liquid sloshing in two-row tanks,” *Journal of Marine Science and Engineering*, 8, 582.

Ji, XJ, Li, Y, Tang, YG, and Tong, B (2019). “Viscous damping effect and vortex shedding performance of the novel anti-motion structures on a cylindrical FPSO,” *Ocean Engineering*, 190, 106430.

Ji, XJ, Li, Y, Tang, YG, Zhu, Q, and Hu, ZQ (2019). “Damping performance of annular anti-motion structures on a cylindrical floating drilling production storage and offloading system,” *Ocean Engineering*, 192, 106590.

Liu, ZH, Zhao, WW, and Wan, DC (2021). “CFD study of wave interaction with single and two tandem circular cylinders,” *Ocean Engineering*, 239, 109855.

Rao, MJ, Seeninaidu, N, and Bhattacharyya, S (2014). " CFD simulation and experimental studies on frequency and amplitude dependency of heave damping of spar hull with and without heave plate," ACEMH 2014, 2, 108-117.

Wu, DK, Wang, JH, and Wan, DC (2021). “Delayed detached eddy simulation method for breaking bow waves of a surface combatant model with different trim angle,” *Ocean Engineering*, 242, 110177.